OPEN ACCESS
Fractals, Vol. 29, No. 5 (2021) 2140017 (15 pages)

DOI: 10.1142/S0218348X2140017X

World Scientific
www.worldscientific.com

FRACTIONAL MAYER NEURO-SWARM HEURISTIC SOLVER FOR MULTI-FRACTIONAL ORDER DOUBLY SINGULAR MODEL BASED ON LANE–EMDEN EQUATION

ZULQURNAIN SABIR,[*,**], MUHAMMAD ASIF ZAHOOR RAJA[†,‡,††] and DUMITRU BALEANU[§,¶,‖,‡‡]

[*]*Department of Mathematics and Statistics*
Hazara University, Mansehra, Pakistan

[†]*Future Technology Research Center*
National Yunlin University of Science and Technology
123 University Road, Section 3 Douliou
Yunlin 64002, Taiwan, R.O.C.

[‡]*Department of Electrical and Computer Engineering*
COMSATS University Islamabad, Attock Campus
Attock 43600, Pakistan

[§]*Department of Mathematics, Cankaya University, Ankara, Turkey*

[¶]*Institute of Space Science, Magurele-Bucharest, Romania*

[††]Corresponding author.

‖*Department of Medical Research*
China Medical University Hospital
China Medical University, Taichung, Taiwan
****zulqurnain_maths@hu.edu.pk*
††*rajamaz@yuntech.edu.tw*
‡‡*dumitru@cankaya.edu.tr*

Received August 2, 2020
Accepted October 26, 2020
Published March 25, 2021

Abstract

This research is related to present a novel fractional Mayer neuro-swarming intelligent solver for the numerical treatment of multi-fractional order doubly singular Lane–Emden (LE) equation using combined investigations of the Mayer wavelet (MW) neural networks (NNs) optimized by the global search effectiveness of particle swarm optimization (PSO) and interior-point (IP) method, i.e. MW-NN-PSOIP. The design of novel fractional Mayer neuro-swarming intelligent solver for multi-fractional order doubly singular LE equation is derived from the standard LE model and the shape factors; fractional order terms along with singular points are examined. The modeling based on the MW-NN strength is implemented to signify the multi-fractional order doubly singular LE model using the ability of mean squared error in terms of the merit function and the networks are optimized with the integrated capability of PSOIP scheme. The perfection, verification and validation of the fractional Mayer neuro-swarming intelligent solver for three different cases of the multi-fractional order doubly singular LE equation are recognized through comparative investigations from the reference results on different measures based on the convergence, robustness, stability and accuracy. Furthermore, the statics interpretations further validate the performance of the proposed fractional Mayer neuro-swarming intelligent solvers.

Keywords: Lane–Emden Multi-fractional Model; Mayer Wavelet Neural Systems; Singular Systems; Particle Swarm Optimization; Artificial Neural Networks; Interior Programming.

1. INTRODUCTION

The fractional order differential system represented with fractional order and integer terms have been broadly investigated due to the numerous applications in control systems, physics, engineering and mathematical sciences. The study of fractional calculus along with different operatives have become an interesting and valued topic for the researchers during the last 30 to 35 years, few paramount implications of these operatives are the Weyl–Riesz operator,[1] the Riemann–Liouville,[2] Grnwald–Letnikov operative[3] and the Erdlyi–Kober operative.[4] Many researchers worked on the importance and significance of these mentioned fractional operatives in diverse fields, like as to model the fractional viscoplasticity,[5,6] dynamical investigations of the earth system,[7] detection of edge in road hurdle,[8] surface–volume reaction models,[9] electromagnetic theory established using the concepts of fractional calculus,[10] LC-electric circuit fractal model,[11] comprehensive performances in the real supplies,[12] viscoelastic model systems,[13] nanofluids mathematical models[14] and many more, see references therein.[15–19]

There are various classes of linear or nonlinear, homogeneous or non-homogeneous, singular or non-singular systems, which are not easy to solve numerically or analytically by using the conventional or traditional schemes, one of the class is the Lane–Emden (LE) that is famous due to singularity at the origin. The LE system occurs in quantum mechanics, astrophysics and spherical gas cloud, etc., which

are considered difficult and stiff to solve due to singular nature. A number of deterministic systems have been functional to solve the LE system[20–26] and its generic form is given as[27–29]

$$\begin{cases} \dfrac{d^2Z}{dX^2} + \dfrac{\lambda}{X}\dfrac{dZ}{dX} \\ \quad + H(Z) = G(X), \quad \lambda \geq 1, \\ Z(0) = A, \qquad\qquad \dfrac{dZ(0)}{dX} = B, \end{cases} \tag{1}$$

where λ is the shape vector form in Eq. (1) with singularity at origin, i.e. $X = 0$. The structure of fractional Mayer neuro-swarm heuristic solver for multi-fractional order doubly singular (MFODS) model based on LE equation, i.e. MFODS-LE equation is given as[30]

$$X^{-\lambda}\frac{d^q}{dX^q}\left(X^{\lambda}\frac{d^s}{dX^s}\right)Z(X) + H(Z) = G(X), \tag{2}$$

where λ is a real positive number. For the derivation of MFODS-LE equation, the values of q and s are defined as

$$q = 2, \quad s = \beta, \quad \text{where } 0 < \beta < 1. \tag{3}$$

The simplified form of Eq. (2) using the values of Eq. (3) is written as

$$X^{-\lambda}\frac{d^2}{dX^2}\left(X^{\lambda}\frac{d^\beta}{dX^\beta}\right)Z(X) + H(Z) = G(X), \tag{4}$$

Simplifying the above equation, we get

$$\begin{aligned} &\frac{d^2}{dX^2}\left(X^{\lambda}\frac{d^\beta}{dX^\beta}\right)Z(X) \\ &\quad = X^{\lambda}\frac{d^{\beta+2}}{dX^{\beta+2}}Z(X) + 2\lambda X^{\lambda-1} \\ &\qquad \times \frac{d^{\beta+1}}{dX^{\beta+1}}Z(X) + \lambda(\lambda-1) \\ &\qquad \times X^{\lambda-2}\frac{d^\beta}{dX^\beta}Z(X). \end{aligned} \tag{5}$$

Consequently, the mathematical model is achieved as

$$\begin{cases} \dfrac{d^{\beta+2}}{dX^{\beta+2}}Z(X) + \dfrac{2\lambda}{X}\dfrac{d^{\beta+1}}{dX^{\beta+1}}Z(X) \\ \quad + \dfrac{\lambda(\lambda-1)}{X^2}\dfrac{d^\beta}{dX^\beta}Z(X) \\ \quad + H(Z) = G(X), \quad Z(0) = 0, \\ \quad Z(1) = 0. \end{cases} \tag{6}$$

The achieved mathematical form given in Eq. (6) is called as MFODS-LE model, the singular-point is noticed twice at the origin at X and X^2, respectively, the values of the shape factors are 2λ and $\lambda(\lambda-1)$ in the second and third factors, while the fractional order is β that appears thrice as β, $\beta+1$ and $\beta+2$. Furthermore, for $\lambda = 1$, the third factor vanishes, and the value of the shape factor becomes 2. The purpose of this research is to design as well as numerically present the solutions of the MFODS-LE model defined in Eq. (6) through the Mayer wavelet (MW) neural networks (NNs), i.e. MWNNs improved with the global search effectiveness of particle swarm optimization (PSO) and interior-point (IP) method, i.e. MW-NN-PSOIP. The novel features of this research are defined into segments as:

(1) A novel design of the MFODS-LE model is described with the derivation procedure using the standard form of the LE system.
(2) Soft computing or machine learning procedures-based novel fractional Mayer neuro-swarm computing intelligent solver has been considered and oppressed to solve the MFODS-LE system.

The numerical procedures through neuro-swarm computational solvers are widely exploited for the investigations of singular or non-singular models represented by linear or nonlinear differential systems using NNs trained with swarming or evolutionary computing techniques.[31–35] Few current implementations of these methods are singular functional differential models,[36,37] singular third-order nonlinear model,[38] prey–predator models,[39] plasma physics model,[40] model of heartbeat dynamics,[41] infectious disease model for HIV infection,[42] singular heat conduction human head-based model,[43] multiple singularity-based nonlinear models,[44] singular atomic physics model of Thomas–Fermi equation,[45] corneal shape model[46] and multi-point boundary value systems.[47] These current contributions inspired the authors to design the novel fractional Mayer neuro-swarming intelligent solver for the mathematical MFODS-LE model. Some noticeable and prominent geographies of proposed novel fractional Mayer neuro-swarming intelligent solver in the form of MW-NN-PSOIP for solving the novel MFODS-LE model are itemized as:

- A novel MFODS-LE model is derived from the fundamental LE system model and effectively treated to get the numerical solutions using the proposed fractional MW-NN-PSOIP method.

- The proposed Mayer neuro-swarming intelligent solver through fractional MW-NN-PSOIP is presented to solve three different singular variants of the MFODS-LE model and comparison of the obtained numerical results from the existing exact/true results validate its stability, correctness and convergence.
- The presentation of the proposed fractional MW-NN-PSOIP method is recognized via the statistical inquiries by means of Theil's inequality coefficient (TIC), semi-interquartile range (SI.R), and variance account for (VAF).
- Beside the soundly accurate results for the MFODS-LE model, smooth operations, ease of understanding, stability, exhaustive applicability and robustness are other valued advantages of the novel fractional Mayer neuro-swarming intelligent solver.

The remaining parts of the paper are reported as follows: The proposed fractional MW-NN-PSOIP methodology is defined in Sec. 2 for solving MFODS-LE model. Performance measures are given in Sec. 3. The details of the results are provided in Sec. 4. The conclusions along with research guidelines are reported in Sec. 5.

2. METHODOLOGY

Fractional Mayer neuro-swarm intelligent-based computational procedure.

This section is associated to present the fractional Mayer neuro-swarm intelligent-based computational mechanism and execution process for the MFODS-LE model using the designed fractional MW-NN-PSOIP for the MW kernels. The construction of error-based fitness/merit function (MF) of the model and its optimization with PSOIP is also described in this section.

2.1. Activation Function: Fractional MW-NNs

The models based on ANN are implemented to provide the numerical solutions of many fractional order models.[51,52] In this procedure, $\hat{Z}(X)$shows the proposed solutions of the designed system, $D^{(n)}\hat{Z}(X)$and $D^{\beta}\hat{Z}(X)$ indicate the nth order integer as well as respective fractional derivative. The network terminologies become mathematically as follows:

$$\begin{aligned}\hat{Z}(X) &= \sum_{i=1}^{r} p_i T(w_i X + q_i),\\ D^{(n)}\hat{Z}(X) &= \sum_{i=1}^{r} p_i D^{(n)} T(w_i X + q_i),\\ D^{\beta}\hat{Z}(X) &= \sum_{i=1}^{r} p_i D^{\beta} T(w_i X + q_i),\end{aligned} \tag{7}$$

where r being a number to represent neurons, p, w and q are the entries of W, as given below:

$$\mathbf{W} = [\mathbf{p}, \mathbf{w}, \mathbf{q}]$$

for $\mathbf{p} = [p_1, p_2, \ldots, p_r]$, $\mathbf{w} = [w_1, w_2, \ldots, w_r]$ and $\mathbf{q} = [q_1, q_2, \ldots, q_r]$. The MW activation/transfer kernel/function is written as follows:

$$T(X) = 35X^4 - 84X^5 + 70X^6 - 20X^7. \tag{8}$$

The modified (7) using Eq. (8) is given as follows:

$$\begin{aligned}&\hat{Z}(X)\\ &= \sum_{i=1}^{r} p_i \begin{pmatrix} 35(w_i X + q_i)^4 \\ -84(w_i X + q_i)^5 \\ +70(w_i X + q_i)^6 \\ -20(w_i X + q_i)^7 \end{pmatrix},\\ &D^{(n)}\hat{Z}(X)\\ &= \sum_{i=1}^{m} p_i \begin{pmatrix} 35D^{(n)}(w_i X + q_i)^4 \\ -84D^{(n)}(w_i X + q_i)^5 \\ +70D^{(n)}(w_i X + q_i)^6 \\ -20D^{(n)}(w_i X + q_i)^7 \end{pmatrix},\\ &D^{\beta}\hat{Z}(X)\\ &= \sum_{i=1}^{m} p_i \begin{pmatrix} 35D^{\beta}(w_i X + q_i)^4 \\ -84D^{\beta}(w_i X + q_i)^5 \\ +70D^{\beta}(w_i X + q_i)^6 \\ -20D^{\beta}(w_i X + q_i)^7 \end{pmatrix}.\end{aligned} \tag{9}$$

The arbitrary ANN combinations with MW kernels is applied for solving the designed novel MFODS-LE model associated with the accessibility of the appropriate weight vector W. In order to evaluate the estimated ANN weights, we use the mean squared error-based MF called E_{Fit} which is

written as follows:

$$E_{\text{Fit}} = E_{\text{Fit}-1} + E_{\text{Fit}-2}, \tag{10}$$

where $E_{\text{Fit}-1}$ and $E_{\text{Fit}-2}$ are the MFs related to the differential equation and boundary conditions of the MFODS-LE model, which are written as follows:

$$E_{\text{Fit}-1} = \frac{1}{N}\sum_{i=1}^{r} \times \left(\begin{array}{l} \dfrac{d^{\beta+2}}{dX^{\beta+2}}\hat{Z}_r \\ \quad + \dfrac{2\lambda}{X_r}\dfrac{d^{\beta+1}}{dX^{\beta+1}}\hat{Z}_r \\ \quad + \dfrac{\lambda(\lambda-1)}{X_r^2}\dfrac{d^{\beta}}{dX^{\beta}}\hat{Z}_r \\ \quad + H(\hat{Z}_r) - G_r \end{array} \right)^2, \tag{11}$$

$$E_{\text{Fit}-2} = \frac{1}{2}((\hat{Z}_0)^2 + (\hat{Z}_N)^2) \tag{12}$$

for

$$Nh = 1, \quad \hat{Z}_r = \hat{Z}(X_r), \quad G_r = G(X_r), \quad X_r = rh.$$

One may define the solution of MFODS-LE model (6) with the obtainability of suitable weights W, such that $E_{\text{Fit}} \to 0$.

2.2. Networks Optimization

The optimization of the parameter for the fractional MW-ANN is achieved by hybrid of PSO and IP, i.e. PSOIP to solve the MFODS-LE model.

2.3. Optimization Using PSOIPA

The computational hybrid character of PSO and IPA, i.e. PSOIPA approves the parameter optimization for solving the second kind of PD model.

PSO is an optimization global search scheme[48] applied broadly as a functioning replacement of the genetic algorithm that is also a global search technique.[49] Kennedy and Eberhart suggested PSO, i.e. a renowned easy implementation global search method and short memory processes required..[50] Few current PSO applications are fuel ignition network,[51] feature arrangements,[52] to balance the U-lines stochastic model,[53] operation procedure of microgrids[54] and physical models based on nonlinearity.[55]

In this study, a single applicant or candidate solution using the process of optimization is called particle of the swarm. To adjust the PSO parameters, the scheme offers optimal solutions $\mathbf{P}_{LB}^{A-1}$ and $\mathbf{P}_{GB}^{A-1}$ iteratively that represents the respective swarm position as well as velocity, which is mathematically written as follows:

$$\mathbf{X}_j^A = \mathbf{X}_j^{A-1} + \mathbf{V}_j^{A-1}, \tag{13}$$

$$\mathbf{V}_j^A = \Upsilon\mathbf{V}_j^{A-1} + A_1(\mathbf{P}_{LB}^{A-1} - \mathbf{X}_j^{A-1})\mathbf{r}_1 + A_2(\mathbf{P}_{GB}^{A-1} - \mathbf{X}_j^{A-1})\mathbf{r}_2, \tag{14}$$

where X_i is the position and V_i is the velocity, A_1 and A_2 are the constant acceleration values.

The process of hybridization of the PSO is implemented for rapidly convergence ability with IP method by taking the best particle of the swarm as a start point. Therefore, a quick and effective local search IP method is applied to adjust the proficient outcomes using the designed MW-NN-PSOIP method. Few current submission of the IP method is the active noise control nets,[56] mixed complementarily monotone nets,[57] reproduction of aircraft parts riveting,[58] nonlinear identification systems[59] and economic load dispatch models.[60]

3. PERFORMANCE INDICES

The performance processes based on the TIC and EVAF are shown in this section. The mathematical notations of TIC and EVAF along with the global demonstrations of Global TIC (G-TIC) and Global EVAF (G-EVAF) have been proposed to solve the MFODS-LE model, mathematically represented as

$$\text{TIC} = \frac{\sqrt{\frac{1}{n}\sum_{j=1}^{n}(Z_j - \hat{Z}_j)^2}}{\left(\sqrt{\frac{1}{n}\sum_{j=1}^{n}Z_j^2} + \sqrt{\frac{1}{n}\sum_{j=1}^{n}\hat{Z}_j^2}\right)}, \tag{15}$$

$$\begin{cases} \text{VAF} = \left(1 - \dfrac{\text{var}(Z_j - \hat{Z}_j)}{\text{var}(Z_j)}\right) \times 100, \\ \text{EVAF} = |\text{VAF} - 100|. \end{cases} \tag{16}$$

4. SIMULATIONS AND RESULTS

The numerical outcomes of the comprehensive simulations to solve three cases based on the MFODS-LE model are provided here. The proposed solver MW-NN-PSOIP results depending on the multiple runs for the MFODS-LE model-based cases are plotted with sufficient graphical and numerical illustrations to assess the accuracy as well as convergence.

Example 1. Consider the MFODS-LE model shown in Eq. (6) which is written as

$$\begin{cases} X^2\dfrac{d^{\beta+2}}{dX^{\beta+2}}Z(X)+4X\dfrac{d^{\beta+1}}{dX^{\beta+1}}Z(X) \\ \quad +2\dfrac{d^{\beta}}{dX^{\beta}}Z(X)+X^2H(Z) \\ \quad =X^2G(X)=J(X), \quad Z(0)=Z(1)=0, \end{cases} \tag{17}$$

where

$$\begin{aligned} J(X)=&X^{q+2}-X^{s+2} \\ &+X^2\left(\frac{\Gamma(q+1)}{\Gamma(q-\beta-1)}X^{q-\beta-2}\right. \\ &\left.-\frac{\Gamma(s+1)}{\Gamma(s-\beta-1)}x^{s-\beta-2}\right) \\ &+4X\left(\frac{\Gamma(q+1)}{\Gamma(q-\beta)}X^{q-\beta-1}\right. \\ &\left.-\frac{\Gamma(s+1)}{\Gamma(s-\beta-1)}X^{s-\beta-1}\right) \\ &+2\left(\frac{\Gamma(q+1)}{\Gamma(q-\beta+1)}x^{q-\beta}\right. \\ &\left.-\frac{\Gamma(s+1)}{\Gamma(s-\beta+1)}x^{s-\beta}\right). \end{aligned} \tag{18}$$

In Eq. (18), q and s are taken as positive. Combining Eqs. (17) and (18), the updated form is written as:

$$\begin{cases} X^2\dfrac{d^{\beta+2}}{dX^{\beta+2}}Z(X)+4X\dfrac{d^{\beta+1}}{dX^{\beta+1}}Z(X) \\ \quad +2\dfrac{d^{\beta}}{dX^{\beta}}Z(X)+X^2H(Z) \\ \quad =X^{q+2}-X^{s+2} \\ \quad +X^2\left(\begin{array}{l}\dfrac{\Gamma(q+1)}{\Gamma(q-\beta-1)}X^{q-\beta-2} \\ -\dfrac{\Gamma(s+1)}{\Gamma(s-\beta-1)}X^{s-\beta-2}\end{array}\right) \\ \quad +4x\left(\begin{array}{l}\dfrac{\Gamma(q+1)}{\Gamma(q-\beta)}X^{q-\beta-1} \\ -\dfrac{\Gamma(s+1)}{\Gamma(s-\beta-1)}x^{s-\beta-1}\end{array}\right) \\ \quad +2\left(\dfrac{\Gamma(q+1)}{\Gamma(q-\beta+1)}X^{q-\beta}\right. \\ \quad \left.-\dfrac{\Gamma(s+1)}{\Gamma(s-\beta+1)}X^{s-\beta}\right), Z(0)=Z(1)=0. \end{cases} \tag{19}$$

The exact solution of the above MFODS-LE model (19) is given as

$$Z(X)=X^q-X^s. \tag{20}$$

Now for the specific values of $q=4$ and $s=3$, the exact solution can be taken the form as

$$Z(X)=X^4-X^3. \tag{21}$$

The MF for Eq. (19) is written as

$$\begin{aligned} E_{\text{Fit}-1}=&\frac{1}{N} \\ &\times\sum_{i=1}^{r}\left(\begin{array}{l} X_i^2\dfrac{d^{\beta+2}}{dx_r^{\beta+2}}\hat{Z}_r \\ \quad +4X\dfrac{d^{\beta+1}}{dX_r^{\beta+1}}\hat{Z}_r+2\dfrac{d^{\beta}}{dX_r^{\beta}}\hat{Z}_r \\ \quad +X_r^2H(\hat{Z}_r)-X_r^{q+2}+X_r^{s+2} \\ \quad -X_r^2\left(\begin{array}{l}\dfrac{24}{\Gamma(3-\beta)}X_r^{2-\beta} \\ -\dfrac{6}{\Gamma(2-\beta)}X_r^{1-\beta}\end{array}\right) \\ \quad -4X_r\left(\begin{array}{l}\dfrac{24}{\Gamma(4-\beta)}X_i^{3-\beta} \\ -\dfrac{6}{\Gamma(3-\beta)}X_r^{2-\beta}\end{array}\right) \\ \quad -2\left(\dfrac{24}{\Gamma(5-\beta)}X_r^{4-\beta}\right. \\ \quad \left.-\dfrac{6}{\Gamma(4-\beta)}X_r^{3-\beta}\right) \end{array}\right)^2 \\ &+\frac{1}{2}((\hat{Z}_0)^2+(\hat{Z}_m)^2). \end{aligned} \tag{22}$$

Three cases for the MFODS-LE model are considered for different values of β, i.e. $\beta=0.2$, 0.5 and 0.8, respectively.

To observe the performance of all the three cases of the MFODS-LE model, optimization is executed by PSOIP method. The entire procedure is repeated for 70 times to produce the parameters of ANNs. These trained ANN weights are applied to the first set of the system (9) to assess the proposed results for all cases of the MFODS-LE model. The mathematical representations accomplished by one set of the optimized factors to design the fractional MW-NN-PSOIP method for all cases of the MFODS-LE

model are written as

$$\begin{aligned}\hat{Z}_{C-1} &= 2.4252 \\ &\quad \times \begin{pmatrix} 35(-0.844X + 0.9955)^4 \\ -84(-0.844X + 0.9955)^5 \\ +70(-0.844X + 0.9955)^6 \\ -20(-0.844X + 0.9955)^7 \end{pmatrix} \\ &\quad -0.2540 \\ &\quad \times \begin{pmatrix} 35(-0.030X - 0.2822)^4 \\ -84(-0.030X - 0.2822)^5 \\ +70(-0.030X - 0.2822)^6 \\ -20(-0.030X - 0.2822)^7 \end{pmatrix} \\ &\quad -0.0175 \\ &\quad \times \begin{pmatrix} 35(0.3751X - 0.5716)^4 \\ -84(0.3751X - 0.5716)^5 \\ +70(0.3751X - 0.5716)^6 \\ -20(0.3751X - 0.5716)^7 \end{pmatrix} \\ &\quad + \cdots - 1.2977 \\ &\quad \times \begin{pmatrix} 35(0.9050X + 0.8468)^4 \\ -84(0.9050X + 0.8468)^5 \\ +70(0.9050X + 0.8468)^6 \\ -20(0.9050X + 0.8468)^7 \end{pmatrix}, \end{aligned} \tag{23}$$

$$\begin{aligned}\hat{Z}_{C-2} &= 0.6909 \\ &\quad \times \begin{pmatrix} 35(-0.793X + 0.9935)^4 \\ -84(-0.793X + 0.9935)^5 \\ +70(-0.793X + 0.9935)^6 \\ -20(-0.793X + 0.9935)^7 \end{pmatrix} \\ &\quad -0.3197 \\ &\quad \times \begin{pmatrix} 35(-0.886X + 1.0407)^4 \\ -84(-0.886X + 1.0407)^5 \\ +70(-0.886X + 1.0407)^6 \\ -20(-0.886X + 1.0407)^7 \end{pmatrix} \\ &\quad -0.5709 \\ &\quad \times \begin{pmatrix} 35(0.1136X - 0.3916)^4 \\ -84(0.1136X - 0.3916)^5 \\ +70(0.1136X - 0.3916)^6 \\ -20(0.1136X - 0.3916)^7 \end{pmatrix} \\ &\quad + \cdots - 1.2977 \\ &\quad \times \begin{pmatrix} 35(0.9050X + 0.8468)^4 \\ -84(0.9050X + 0.8468)^5 \\ +70(0.9050X + 0.8468)^6 \\ -20(0.9050X + 0.8468)^7 \end{pmatrix}, \end{aligned} \tag{24}$$

$$\begin{aligned}\hat{Z}_{C-3} &= -0.032 \\ &\quad \times \begin{pmatrix} 35(0.0823X + 1.6275)^4 \\ -84(0.0823X + 1.6275)^5 \\ +70(0.0823X + 1.6275)^6 \\ -20(0.0823X + 1.6275)^7 \end{pmatrix} \\ &\quad -0.0204 \\ &\quad \times \begin{pmatrix} 35(-0.974X + 1.1694)^4 \\ -84(-0.974X + 1.1694)^5 \\ +70(-0.974X + 1.1694)^6 \\ -20(-0.974X + 1.1694)^7 \end{pmatrix} \\ &\quad -0.7684 \\ &\quad \times \begin{pmatrix} 35(0.3340X - 0.8961)^4 \\ -84(0.3340X - 0.8961)^5 \\ +70(0.3340X - 0.8961)^6 \\ -20(0.3340X - 0.896)^7 \end{pmatrix} \\ &\quad + \cdots + 1.2977 \\ &\quad \times \begin{pmatrix} 35(0.0969X + 0.3591)^4 \\ -84(0.0969X + 0.3591)^5 \\ +70(0.0969X + 0.3591)^6 \\ -20(0.0969X + 0.3591)^7 \end{pmatrix}. \end{aligned} \tag{25}$$

The approximate outcomes obtained by the MW-NN-PSOIP are represented in Eqs. (23)–(25) and these obtained numerical outcomes are graphically established in Figs. 1a–1c for all cases of the MFODS-LE model. The comparison of three solutions best, worst and mean is provided in Figs. 1d–1f for all cases of the MFODS-LE model. It is observed that the best, worst and mean outcomes overlapped to each other. This exact assessment of the numerical outcomes designates the perfection of the proposed MW-NN-PSOIP method. The absolute error (AE) are plotted in Fig. 1g for all cases of the MFODS-LE model. It is depicted that the AE for Cases 1–3, lie in the range of 10^{-07}–10^{-09}, 10^{-07}–10^{-08} and 10^{-08}–10^{-10}, respectively. The span of the performance investigations in terms

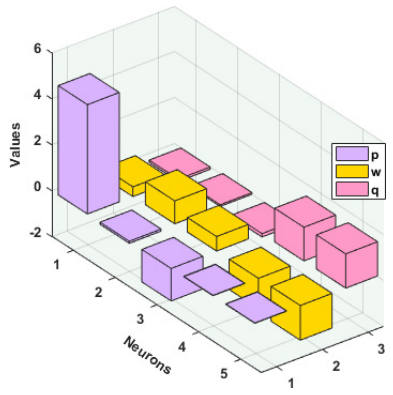

(a) Weight of NNs for MFODS-LE: Case 1

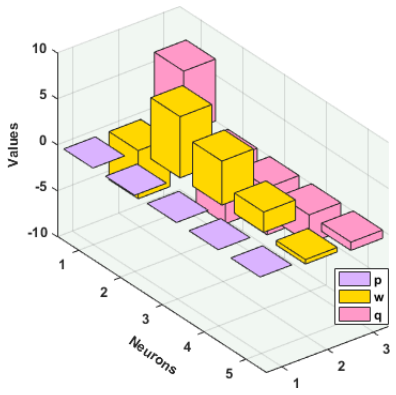

(b) Weight of NNs for MFODS-LE: Case 2

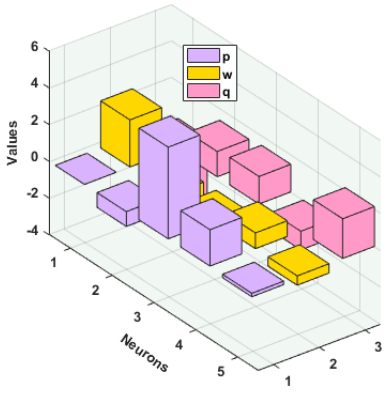

(c) Weight of NNs for MFODS-LE: Case 3

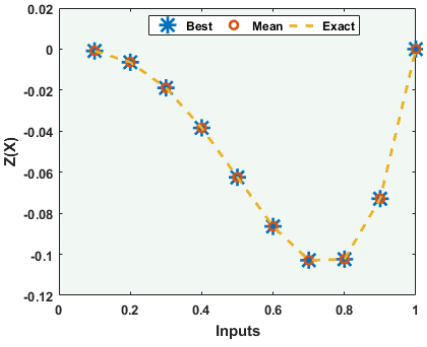

(d) Results of MFODS-LE model: Case 1

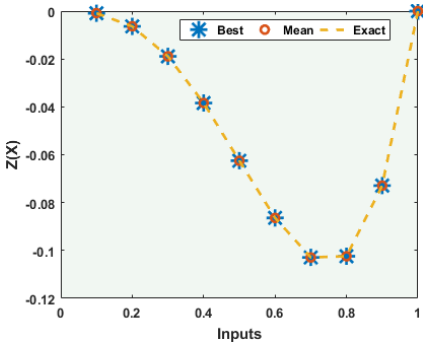

(e) Results of MFODS-LE model: Case 2

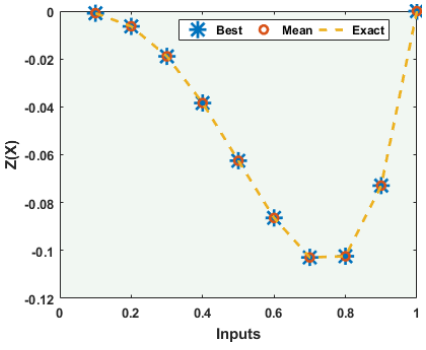

(f) Results of MFODS-LE model: Case 3

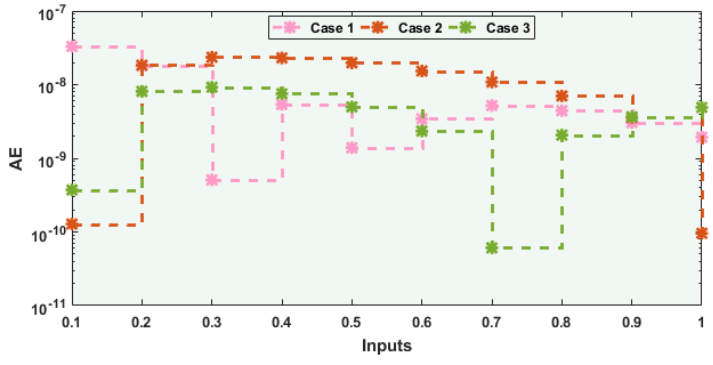

(g) AE for all the cases of MFODS-LE system

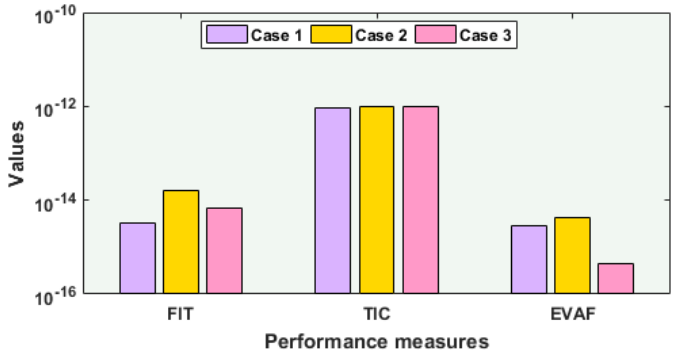

(h) Performance studies for all the cases of MFODS-LE system

Fig. 1 Outcomes of proposed scheme (a)–(c), weight sets (d)–(f), AE values (g) and performance studies (h).

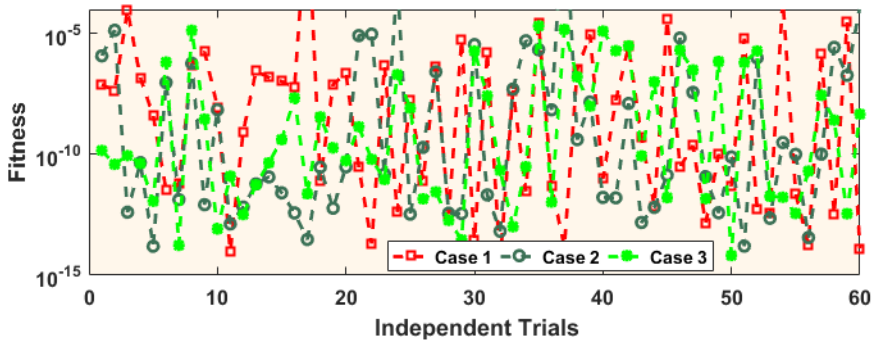

(a) Fitness values in convergence investigations for Cases 1–3

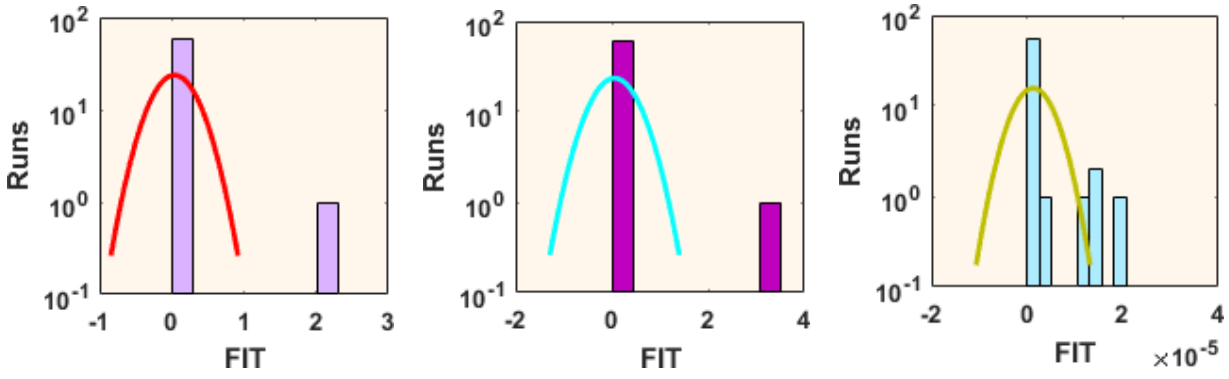

(b) Histogram: Case 1 **(c)** Histogram: Case 2 **(d)** Histogram: Case 3

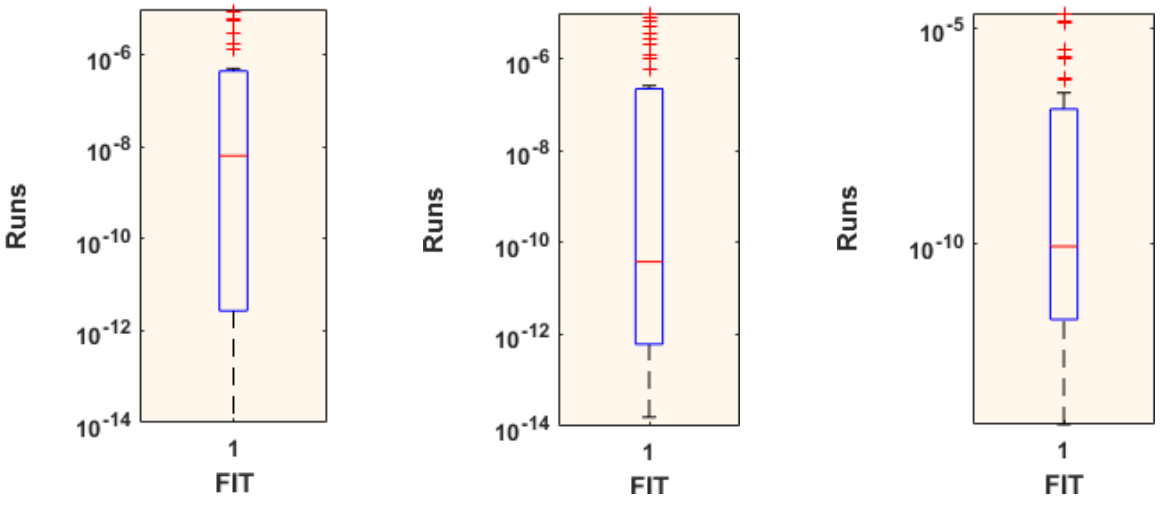

(e) Boxplot: Case 1 **(f)** Boxplot: Case 2 **(g)** Boxplot: Case 3

Fig. 2 Statistical performance of the MW-NN-PSOIP method via Fitness values along with histogram and box plots for all the cases of MFODS-LE system.

of Fitness, TIC and EVAF values is provided in Fig. 1h for all cases of the MFODS-LE model. It is observed that the best fitness for Cases 1–3 are closely lying around 10^{-14}–10^{-16}, 10^{-13}–10^{-14} and 10^{-14} –10^{-15}, respectively. The TIC values for all the cases of the MFODS-LE model lie around 10^{-12}–10^{-13}. Furthermore, the EVAF values for all the cases of the MFODS-LE model lie in the range of 10^{-14}–10^{-16}.

The performance practices for the Fitness, EVAF and TIC together with the histogram values and box plots are drawn in Figs. 2–4 for all cases of the

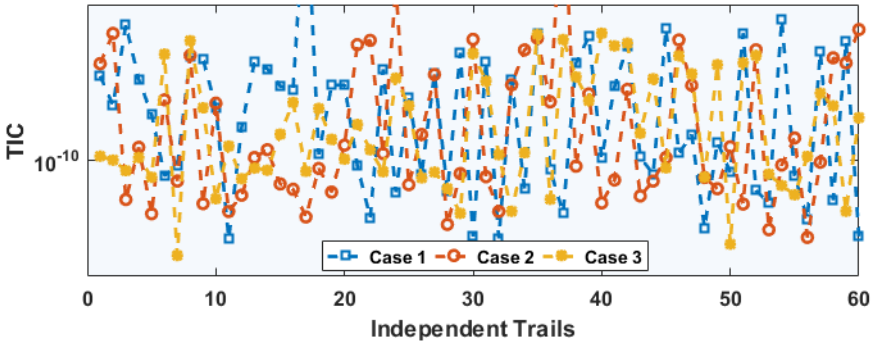

(a) TIC values in convergence investigations for Cases 1– 3

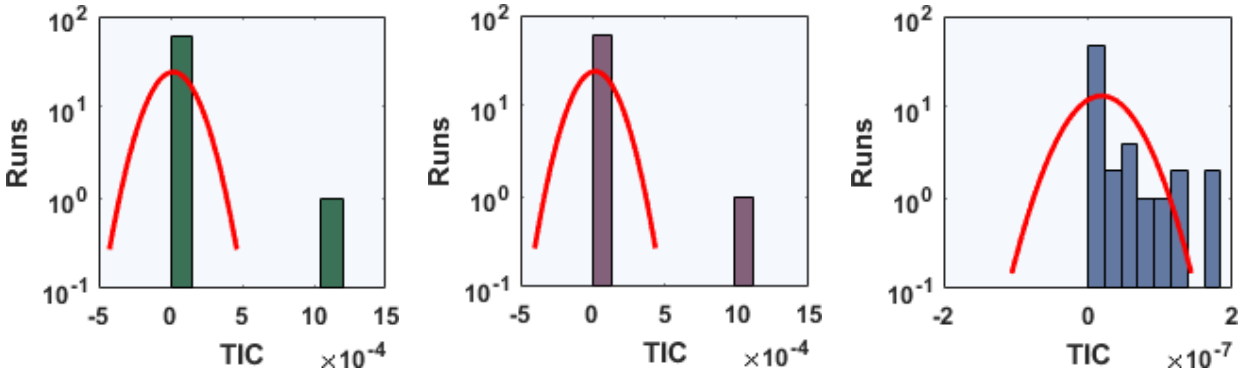

(b) Histogram: Case 1 **(c)** Histogram: Case 2 **(d)** Histogram: Case 3

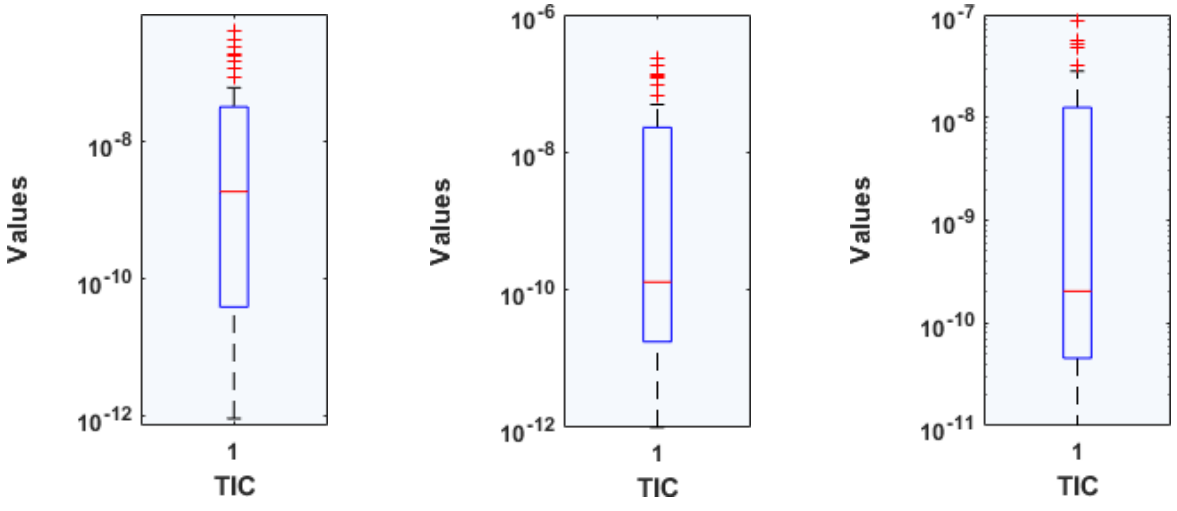

(e) Boxplot: Case 1 **(f)** Boxplot: Case 2 **(g)** Boxplot: Case 3

Fig. 3 Statistical performance of the MW-NN-PSOIP method via TIC along with histograms as well as boxplots for all the cases of MFODS-LE system.

MFODS-LE system. It is depicted that the values of the Fitness, TIC and EVAF for all the cases of the MFODS-LE system lie around 10^{-05}–10^{-13}, 10^{-05}–10^{-12} and 10^{-05}–10^{-13}. On the behalf of these statistical values, one can undertake that the designed MW-NN-PSOIP scheme is accurate and precise.

For the precision and accuracy investigations, the statistical gages through MINimum (Min), Median, MAXimum (Max), Mean, SIR and standard deviation (ST.D) are calculated for 60 times execution of the designed MW-NN-PSOIP and outcomes are shown in Table 1 for the MFODS-LE model-based

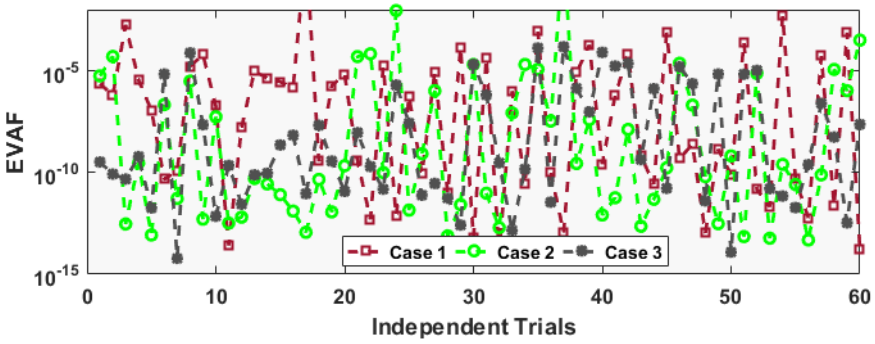

(a) EVAF values in convergence investigations for Cases 1–3

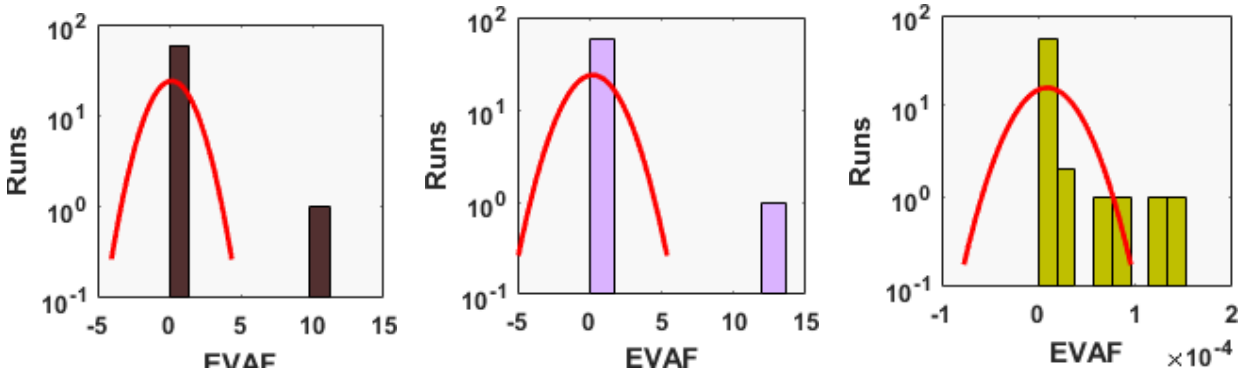

(b) Histogram: Case 1 **(c)** Histogram: Case 2 **(d)** Histogram: Case 3

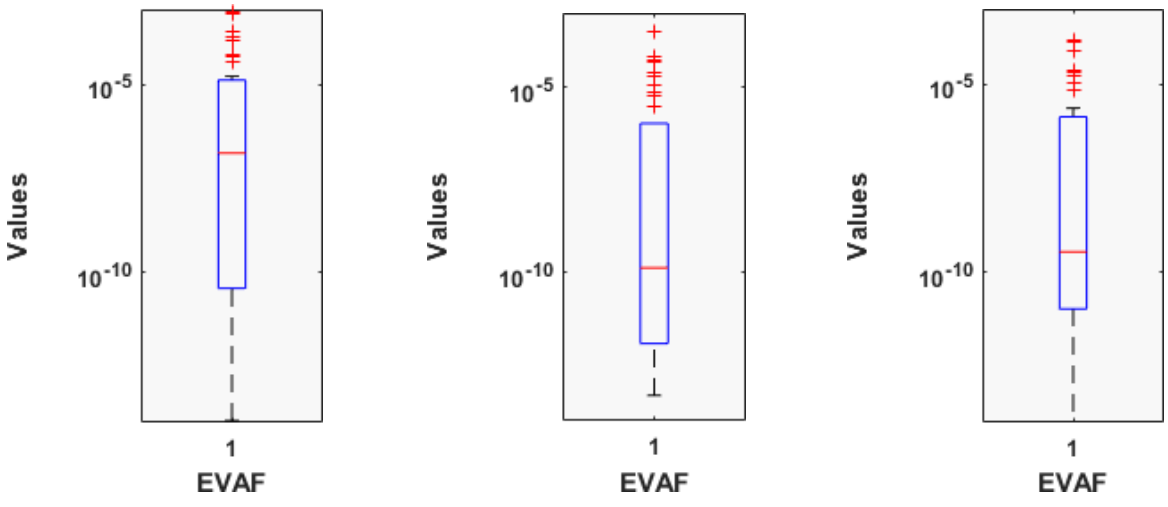

(e) Boxplot: Case 1 **(f)** Boxplot: Case 2 **(g)** Boxplot: Case 3

Fig. 4 Statistical performance of the MW-NN-PSOIP method via EVAF values along with histogram and boxplots for all the cases of MFODS-LE system.

Cases 1–3. The independent trials of the proposed MW-NN-PSOIP solver based on Min and Max values are known as the best and worst executions, respectively. SI.R is the one half of the first and third quartiles. The desired small levels of all the operators, i.e., Min, Median, Max, Mean, ST.D and SI.R authenticate the performance, stability and accuracy of the proposed fractional MW-NN-PSOIP scheme for solving all cases of the MFODS-LE model. To check the convergence of the fractional MW-NN-PSOIP scheme, the global performance in terms of G.FIT, G.TIC and G.EVAF for 60 independent runs to solve the MFODS-LE system is tabulated in Table 2. It is seen that

Table 1 Outcomes of Statistical Investigations for MW-NN-PSOIP in Case of the MFODS-LE Model.

Index	Mode	$Z(X)$for Inputs X									
		0.1	**0.2**	**0.3**	**0.4**	**0.5**	**0.6**	**0.7**	**0.8**	**0.9**	**1**
1	**Min**	2.60E−09	9.40E−12	5.10E−10	2.70E−09	1.40E−09	3.40E−09	5.20E−09	4.40E−09	3.10E−09	1.90E−09
	Max	1.00E−02	1.70E−02	3.70E−02	7.00E−02	1.10E−01	1.60E−01	2.20E−01	2.80E−01	3.50E−01	3.80E−01
	Median	5.30E−05	4.60E−05	2.40E−05	1.50E−05	1.20E−05	1.10E−05	8.50E−06	4.10E−06	3.50E−06	4.50E−06
	Mean	8.30E−04	9.20E−04	1.00E−03	1.50E−03	2.10E−03	3.00E−03	3.80E−03	4.80E−03	5.90E−03	6.40E−03
	SI.R	2.50E−04	2.30E−04	1.50E−04	1.10E−04	9.80E−05	8.60E−05	7.10E−05	5.80E−05	5.00E−05	4.30E−05
	ST.D	1.90E−03	2.60E−03	4.90E−03	9.0E−03	1.40E−02	2.10E−02	2.80E−02	3.60E−02	4.50E−02	4.80E−02
2	**Min**	1.30E−10	1.80E−08	2.2E−09	2.30E−08	1.70E−08	1.10E−08	1.10E−08	7.00E−09	3.60E−09	9.60E−11
	Max	2.10E−02	2.60E−02	3.90E−02	7.30E−02	1.10E−01	1.70E−01	2.40E−01	3.10E−01	3.70E−01	4.20E−01
	Median	1.90E−06	2.40E−06	2.00E−06	1.70E−06	1.70E−06	1.60E−06	1.50E−06	1.30E−06	1.20E−06	1.10E−06
	Mean	7.20E−04	1.00E−03	1.30E−03	1.80E−03	2.50E−03	3.40E−03	4.50E−03	5.50E−03	6.60E−03	7.40E−03
	SI.R	1.20E−04	1.40E−04	1.20E−04	1.10E−04	1.10E−04	9.90E−05	9.10E−05	8.40E−05	7.80E−05	7.30E−05
	ST.D	2.80E−03	4.00E−03	5.80E−03	9.70E−03	1.50E−02	2.30E−02	3.10E−02	3.90E−02	4.80E−02	5.40E−02
3	**Min**	3.70E−10	4.00E−09	8.50E−10	4.00E−09	5.00E−09	2.30E−09	6.10E−11	2.10E−09	3.70E−09	4.90E−09
	Max	5.00E−04	1.40E−03	1.70E−03	1.80E−03	2.00E−03	2.00E−03	2.10E−03	2.10E−03	2.10E−03	2.10E−03
	Median	1.70E−06	2.50E−06	2.60E−06	2.80E−06	3.00E−06	3.10E−06	3.10E−06	2.90E−06	2.90E−06	2.80E−06
	Mean	5.20E−05	1.40E−04	1.70E−04	1.90E−04	2.00E−04	2.10E−04	2.20E−04	2.20E−04	2.20E−04	2.20E−04
	SI.R	2.30E−05	6.30E−05	7.80E−05	8.50E−05	9.10E−05	9.50E−05	9.70E−05	9.80E−05	9.90E−05	9.90E−05
	ST.D	1.10E−04	3.00E−04	3.70E−04	4.10E−04	4.40E−04	4.60E−04	4.60E−04	4.70E−04	4.70E−04	4.70E−04

Table 2 Global Measures for All Cases of the MFODS-LE Model.

Case	G.FIT		G.TIC		G.EVAF	
	Min	**SI.R**	**Min**	**SI.R**	**Min**	**SI.R**
1	3.34998E−15	2.24432E−07	9.22705E−13	1.60408E−08	1.11022E−14	6.48665E−06
2	1.57893E−14	1.12123E−07	1.00447E−12	1.14505E−08	4.84057E−14	5.24990E−07
3	6.58516E−15	6.56010E−08	3.44520E−13	6.23001E−09	5.99520E−15	6.74192E−08

the Min values of the G.FIT, G.TIC and G.EVAF lie closed to 10^{-14}–10^{-15}, 10^{-12}–10^{-13} and 10^{-14}–10^{-15}, while the S.IR for these performances lies around 10^{-07}–10^{-08}, 10^{-08}–10^{-09} and 10^{-06}–10^{-08} for solving MFODS-LE model-based Cases 1–3. The ideal close values of the global operators further validate the accuracy of the proposed fractional MW-NN-PSOIP scheme.

5. CONCLUSION AND UPCOMG RELATED RESEARCH

In this work, multi-fractional doubly singular nonlinear LE system is developed by implementing the idea of the generic form of the LE system. The fractional factor, shape factors and the singular-based points are also reported in the modeled equations. It is observed that the singular points appear twice. The shape factor appears single both in the LE standard form as well as in the present modeling work. To access the perfection of the designed novel multi-fractional LE system, three cases have been implemented and their numerical performance has been investigated using the influential ANNs along with PSO and IP method. The fractional MW-NN-PSOIP method is broadly executed on multi-fractional LE system for three variants to demonstrate the robustness, accuracy and stability. The achieved numerical outcomes from the fractional MW-NN-PSOIP method are compared with the exact outcomes with precision around 7–9 decimal points of accuracy, which validates the perfection as well as efficiency. Furthermore, statistical assessments of the suggested fractional MW-NN-PSOIP method on 70 executions give accurate and precise numerical outcomes. Subsequently, the suggested fractional MW-NN-PSOIP method is not only prominent for smooth viable/operational results, but also one can extend and apply the said scheme with ease.

In the future, one can explore the MW-NN-PSOIP method-based novel fractional Mayer

Neuro-swarming intelligent solver for differential equations containing integer as well as fractional order representation of the variables.

REFERENCES

1. S. Momani and R. W. Ibrahim, On a fractional integral equation of periodic functions involving Weyl–Riesz operator in Banach algebras, *J. Math. Anal. Appl.* **339**(2) (2008) 1210–1219.
2. F. Yu *et al.*, Integrable coupling system of fractional soliton equation hierarchy, *Phys. Lett. A* **373**(41) (2009) 3730–3733.
3. B. Bonilla, M. Rivero and J. J. Trujillo, On systems of linear fractional differential equations with constant coefficients, *Appl. Math. Comput.* **187**(1) (2007) 68–78.
4. K. Diethelm and J. J. Ford, Analysis of fractional differential equations, *J. Math. Anal. Appl.* **265**(2) (2002) 229–248.
5. K. Diethelm and A. D. Freed, On the solution of nonlinear fractional-order differential equations used in the modeling of viscoplasticity, in *Scientific Computing in Chemical Engineering II* (Springer, Berlin, 1999), pp. 217–224.
6. W. Sumelka, Fractional viscoplasticity, *Mech. Res. Commun.* **56** (2014) 31–36.
7. Y. Zhang, H. Sun, H. H. Stowell, M. Zayernouri and S. E. Hansen, A review of applications of fractional calculus in Earth system dynamics, *Chaos Solitons Fractals* **102** (2017) 29–46.
8. R. A. Z. Daou, F. El Samarani, C. Yaacoub and X. Moreau, Fractional derivatives for edge detection: Application to road obstacles, in Smart Cities Performability, Cognition, & Security (Springer, Cham, 2020), pp. 115–137.
9. R. M. Evans, U. N. Katugampola and D. A. Edwards, Applications of fractional calculus in solving Abel-type integral equations: Surface–volume reaction problem, *Comput. Math. Appl.* **73**(6) (2017) 1346–1362.
10. N. Engheia, On the role of fractional calculus in electromagnetic theory, *IEEE Anten. Propag. Mag.* **39**(4) (1997) 35–46.
11. X. J. Yang, J. T. Machado, C. Cattani and F. Gao, On a fractal LC-electric circuit modeled by local fractional calculus, *Commun. Nonlinear Sci. Numer. Simul.* **47** (2017) 200–206.
12. P. J. Torvik and R. L. Bagley, On the appearance of the fractional derivative in the behavior of real materials, *J. Appl. Mech.* **51**(2) (1984) 294–298.
13. M. A. Matlob and Y. Jamali, The concepts and applications of fractional order differential calculus in modeling of viscoelastic systems: A primer, *Crit. Rev. Biomed. Eng.* **47**(4) (2019) 249–276.
14. S. Aman, I. Khan, Z. Ismail and M. Z. Salleh, Applications of fractional derivatives to nanofluids: Exact and numerical solutions, *Math. Model. Nat. Phenom.* **13**(1) (2018) 2.
15. S. Mishra, L. N. Mishra, R. K. Mishra and S. Patnaik, Some applications of fractional calculus in technological development, *J. Fract. Calculus Appl.* **10**(1) (2019) 228–235.
16. H. Sun, Y. Zhang, D. Baleanu, W. Chen and Y. Chen, A new collection of real world applications of fractional calculus in science and engineering, *Commun. Nonlinear Sci. Numer. Simul.* **64** (2018) 213–231.
17. D. Zhao, X. Pan and M. Luo, A new framework for multivariate general conformable fractional calculus and potential applications, *Physica A* **510** (2018) 271–280.
18. I. Jaradat, M. Al-Dolat, K. Al-Zoubi and M. Alquran, Theory and applications of a more general form for fractional power series expansion, *Chaos Solitons Fractals* **108** (2018) 107–110.
19. Y. Zhang, X. Yang, C. Cattani, Z. Dong, T. Yuan and L. Han, Theory and applications of fractional fourier transform and its variants, *Fundam. Inform.* **151**(1–4) (2017) 9–16.
20. Z. Sabir, H. Günerhan and J. L. Guirao, On a new model based on third-order nonlinear multisingular functional differential equations, *Math. Probl. Eng.* **2020** (2020) 1683961, https://doi.org/10.1155/2020/1683961.
21. J. H. He and F. Y. Ji, Taylor series solution for Lane–Emden equation, *J. Math. Chem.* **57**(8) (2019) 1932–1934.
22. R. Singh, J. Shahni, H. Garg and A. Garg, Haar wavelet collocation approach for Lane–Emden equations arising in mathematical physics and astrophysics, *Eur. Phys. J. Plus* **134**(11) (2019) 548.
23. R. Singh, H. Garg and V. Guleria, Haar wavelet collocation method for Lane–Emden equations with Dirichlet, Neumann and Neumann–Robin boundary conditions, *J. Comput. Appl. Math.* **346** (2019) 150–161.
24. W. Adel and Z. Sabir, Solving a new design of nonlinear second-order Lane–Emden pantograph delay differential model via Bernoulli collocation method, *Eur. Phys. J. Plus* **135**(6) (2020) 427.
25. B. Căruntu, C. Bota, M. Lăpădat and M. S. Paşca, Polynomial least squares method for fractional Lane–Emden equations, *Symmetry* **11**(4) (2019) 479.
26. A. S. Khalifa and H. N. Hassan, Approximate solution of Lane–Emden ype equations using variation of parameters method with an auxiliary parameter, *J. Appl. Math. Phys.* **7**(4) (2019) 921.
27. Z. Sabir, F. Amin, D. Pohl and J. L. Guirao, Intelligence computing approach for solving second order

system of Emden–Fowler model, *J. Intell. Fuzzy Syst.* **38**(6) (2020) 7391–7406.
28. M. U. Farooq, Noether-Like operators and first integrals for generalized systems of Lane–Emden equations, *Symmetry* **11**(2) (2019) 162.
29. Z. Sabir, H. A. Wahab, M. Umar, M. G. Sakar and M. A. Z. Raja, Novel design of Morlet wavelet neural network for solving second order Lane–Emden equation, *Math. Comput. Simul.* **172** (2020) 1–14.
30. A. M. Wazwaz, Solving two Emden–Fowler type equations of third order by the variational iteration method, *Appl. Math. Inform. Sci.* **9**(5) (2015) 2429.
31. A. H. Bukhari, M. Sulaiman, S. Islam, M. Shoaib, P. Kumam and M. A. Z. Raja, Neuro-fuzzy modeling and prediction of summer precipitation with application to different meteorological stations, *Alexan, Eng. J.* **59**(1) (2020) 101–116.
32. M. A. Z. Raja, R. Samar, M. A. Manzar and S. M. Shah, Design of unsupervised fractional neural network model optimized with interior point algorithm for solving Bagley–Torvik equation, *Math. Comput. Simul.* **132** (2017) 139–158.
33. W. Waseem, M. Sulaiman, S. Islam, P. Kumam, R. Nawaz, M. A. Z. Raja, M. Farooq and M. Shoaib, A study of changes in temperature profile of porous fin model using cuckoo search algorithm, *Alexan. Eng. J.* **59**(1) (2020) 11–24.
34. I. Ahmad, H. Ilyas, A. Urooj, M. S. Aslam, M. Shoaib and M. A. Z. Raja, Novel applications of intelligent computing paradigms for the analysis of nonlinear reactive transport model of the fluid in soft tissues and microvessels, *Neural Comput. Appl.* **31**(12) (2019) 9041–9059.
35. S. Lodhi, M. A. Manzar and M. A. Z. Raja, Fractional neural network models for nonlinear Riccati systems, *Neural Comput. Appl.* **31**(1) (2019) 359–378.
36. Z. Sabir, M. A. Z. Raja, M. Umar and M. Shoaib, Neuro-swarm intelligent computing to solve the second-order singular functional differential model, *Eur. Phys. J. Plus* **135**(6) (2020) 474.
37. Z. Sabir, H. A. Wahab, M. Umar and F. Erdoğan, Stochastic numerical approach for solving second order nonlinear singular functional differential equation, *Appl. Math. Comput.* **363** (2019) 124605.
38. Z. Sabir, M. A. Z. Raja, M. Umar and M. Shoaib, Design of neuro-swarming-based heuristics to solve the third-order nonlinear multi-singular Emden–Fowler equation, *Eur. Phys. J. Plus* **135**(6) (2020) 410.
39. M. Umar *et al.*, Intelligent computing for numerical treatment of nonlinear prey–predator models, *Appl. Soft Comput.* **80** (2019) 506–524.
40. M. A. Z. Raja, F. H. Shah, M. Tariq and I. Ahmad, Design of artificial neural network models optimized with sequential quadratic programming to study the dynamics of nonlinear Troesch's Example arising in plasma physics, *Neural Comput. Appl.* **29**(6) (2018) 83–109.
41. M. A. Z. Raja, F. H. Shah, E. S. Alaidarous and M. I. Syam, Design of bio-inspired heuristic technique integrated with interior-point algorithm to analyze the dynamics of heartbeat model, *Appl. Soft Comput.* **52** (2017) 605–629.
42. M. Umar, Z. Sabir, F. Amin, J. L. Guirao and M. A. Z. Raja, Stochastic numerical technique for solving HIV infection model of CD4+ T cells, *Eur. Phys. J. Plus* **135**(6) (2020) 403.
43. M. A. Z. Raja, M. Umar, Z. Sabir, J. A. Khan and D. Baleanu, A new stochastic computing paradigm for the dynamics of nonlinear singular heat conduction model of the human head, *Eur. Phys. J. Plus* **133**(9) (2018) 364.
44. M. A. Z. Raja, J. Mehmood, Z. Sabir, A. K. Nasab and M. A. Manzar, Numerical solution of doubly singular nonlinear systems using neural networks-based integrated intelligent computing, *Neural Comput. Appl.* **31**(3) (2019) 793–812.
45. Z. Sabir, M. A. Manzar, M. A. Z. Raja, M. Sheraz and A. M. Wazwaz, Neuro-heuristics for nonlinear singular Thomas–Fermi systems, *Appl. Soft Comput.* **65** (2018) 152–169.
46. M. Umar, F. Amin, H. A. Wahab and D. Baleanu, Unsupervised constrained neural network modeling of boundary value corneal model for eye surgery, *Appl. Soft Comput.* **85** (2019) 105826.
47. Z. Sabir and M. Raja, Numeric treatment of nonlinear second order multi-point boundary value Examples using ANN, GAs and sequential quadratic programming technique, *Int. J. Indus. Eng. Comput.* **5**(3) (2014) 431–442.
48. Y. Shi and R. C. Eberhart, Empirical study of particle swarm optimization, in *Proceedings of the* 1999 *Congress on Evolutionary Computation-CEC99* (*Cat. No. 99TH8406*), Vol. 3 (IEEE, 1999).
49. Y. Shi, Particle swarm optimization: Developments, applications and resources, in *Proceedings of the* 2001 *Congress on Evolutionary Computation* (*IEEE Cat. No. 01TH8546*), Vol. 1 (IEEE, 2001).
50. A. P. Engelbrecht, *Computational Intelligence*: *An Introduction* (John Wiley & Sons, 2007).
51. M. A. Z. Raja, Solution of the one-dimensional Bratu equation arising in the fuel ignition model using ANN optimised with PSO and SQP, *Connect. Sci.* **26**(3) (2014) 195–214.
52. R. A. Ibrahim, A. A. Ewees, D. Oliva, M. A. Elaziz and S. Lu, Improved salp swarm algorithm based on particle swarm optimization for feature selection, *J.*

Amb. Intell. Human. Comput. **10**(8) (2019) 3155–3169.

53. E. K. Aydoğan, Y. Delice, U. Özcan, C. Gencer and Ö. Bali, Balancing stochastic U-lines using particle swarm optimization, *J. Intell. Manufac.* **30**(1) (2019) 97–111.
54. H. Takano, H. Asano and N. Gupta, Application example of particle swarm optimization on operation scheduling of microgrids, in *Frontier Applications of Nature Inspired Computation* (Springer, Singapore, 2020), pp. 215–239.
55. M. A. Z. Raja, A. Zameer, A. K. Kiani, A. Shehzad and M. A. R. Khan, Nature-inspired computational intelligence integration with Nelder–Mead method to solve nonlinear benchmark models, *Neural Comput. Appl.* **29**(4) (2018) 1169–1193.
56. M. A. Z. Raja, M. S. Aslam, N. I. Chaudhary and W. U. Khan, Bio-inspired heuristics hybrid with interior-point method for active noise control systems without identification of secondary path, *Front. Inform. Technol. Electron. Eng.* **19**(2) (2018) 246–259.
57. M. R. Sicre and B. F. Svaiter, An $O(1/k3/2)$ hybrid proximal extragradient primal-dual interior point method for non-linear monotone complementarity problems, Preprint A735/2013, IMPA-Instituto Nacional de Matemtica Pura e Aplicada, Estrada Dona Castorina, 110, pp. 22460–320.
58. M. Stefanova, S. Yakunin, M. Petukhova, S. Lupuleac and M. Kokkolaras, An interior-point method-based solver for simulation of aircraft parts riveting, *Eng. Optim.* **50**(5) (2018) 781–796.
59. J. Umenberger and I. R. Manchester, Specialized interior-point algorithm for stable nonlinear system identification, *IEEE Trans. Autom. Control* **64**(6) (2018) 2442–2456.
60. M. A. Z. Raja, U. Ahmed, A. Zameer, A. K. Kiani and N. I. Chaudhary, Bio-inspired heuristics hybrid with sequential quadratic programming and interior-point methods for reliable treatment of economic load dispatch problem, *Neural Comput. Appl.* **31**(1) (2019) 447–475.